ANALYSIS OF A TENSION MEMBRANE HYPAR ROOF SUBJECTED TO FLUCTUATING WIND LOADS

By P.K.F. Pun and C.W. Letchford

Department of Civil Engineering
University of Queensland, Australia

1 Introduction

Tension membrane structures can be thought of as thin prestressed fabric surfaces. Like cable net structures, tension membrane structures carry and transmit loads by direct tensile stress without bending or compression. They are large displacement structures that rely on geometrical stiffness and prestress to resist loads. The prestress is achieved either by using edge cables or pneumatics. Edge prestressed structures assume anticlastic shapes. A common anticlastic shape is that of the hyperbolic paraboloid, or hypar, which is a doubly curved saddle shape (Fig.1).

In warmer climates, the dominant loading for tension membrane structures is wind, due to their flexibility, light weight and large span, the very characteristics that make them so appealing. Yet, not much is known about the wind loads on these structures because of the uniqueness of each individual structure. This study aims to characterise the wind loads on a tension membrane hypar and to estimate the peak load effects of the structure due to wind load. The prototype is a free-standing 15mx15m in plan hypar roof. The curvature of the hypar is set by two high support points 7.5m high and two low support points 5m high. Using wind loads determined from boundary layer wind tunnel tests, estimates of the peak reactions at the corner supports were determined with the aid of the non-linear finite element package SHAPE. The covariance integration method was used for these estimates in order to obtain a more accurate description of the fluctuating load effects than that produced using the highly conservative quasi-steady method recommended by most wind codes.

2 Wind Tunnel Tests

The wind tunnel tests were carried out in a 3mx2mx12m recirculating type boundary layer wind tunnel at the University of Queensland. All tests were carried out in a simulated Terrain Category 3 atmospheric boundary layer at a length scale of 1:100 and a velocity scale of 1:2. The boundary layer was formed using roughness elements upstream of the model and a grid and fence at the upstream end of the tunnel.

A rigid 1:100 scale model of the hypar was used. The model was made using two 2mm thick layers of perspex sandwiching a 1.5mm thick acrylic sheet. Eight pockets or manifolds were machined out from both the top and bottom perspex layers, each top and bottom pocket corresponding to a patch on the hypar as shown in Figure 2. Eight pressure tappings were made in each pocket, the tapping locations being chosen as the centroids of equal area triangles subdividing each patch. This arrangement for pressure measurement amounts to an area-averaging technique, which takes into account the spatial correlation of pressures over the patches.

PVC tubes transmit the pressures in each manifold to pressure transducers via Scanivalve switches. The model was mounted on a turntable in the wind tunnel with the

transducers and switches fixed beneath. The Scanivalve switches allowed top and bottom manifold pressures from each patch to be sent in turn to the transducers. The signals from the transducers were analog differenced to obtain nett (top-bottom) pressure differences on the roof. The signals were low pass filtered at 100Hz and sampled at 250Hz for 30s by a high speed data acquisition system.

Area averaged pressures were measured for the hypar to obtain mean, RMS and peak pressure coefficients for angles of attack from 0° to 90° in steps of 15°. The coefficients are referenced to the eaves dynamic pressure with eaves height at the level of the low support points of the hypar (5cm model height). Point pressure measurements were also obtained. Cross correlation coefficients for the patches were obtained using a spectrum analyser. As well as this, area averaged measurements were obtained with 40% and 60% blockages located underneath the hypar and for a grouped arrangement of four hypars. Oil surface flow visualisation tests were also conducted on models of 1.5mm and 6.0mm thicknesses to determine whether the incorrectly scaled thickness of the model would significantly affect the flow patterns and therefore the pressure measurements.

For the 0° angle of attack (Fig.3), high negative panel pressures were measured on panels adjacent to the windward high point, indicating the presence of conical vortices on the top surface edges near this high point. This was confirmed by the point pressure measurements and the flow visualisation tests. Flow over the rest of the surface was attached. For the 90° angle of attack, by symmetry, the vortices formed on the edges adjacent to the windward low point on the bottom surface. However these vortices were much weaker than the ones on the top surface at 0° because the velocity at the level of the low points (eaves height) was much smaller than that at the level of the high points.

The highest single mean panel pressure was found to be at 45° on panel A. However, the most severe overall loading would seem to occur near 0° with large opposing pressures occurring at the front and back of the roof or near 90° with large nett upward pressures over nearly the entire roof.

3 Structural Analysis

The structural analysis of the tension membrane hypar roof was carried out using the 'SHAPE' package. SHAPE is a non-linear finite element analysis package developed by Meek and Ho [1] for shape-finding and membrane analysis of shell and membrane structures.

Once a satisfactory shape of the hypar roof had been determined, load analysis was carried out on it. Fabric exhibits complex biaxial and non-linear stress-strain behaviour. Elastic properties of fabric differ in the warp and weft directions of weave. For this analysis, the SHAPE program was modified to accommodate an orthotropic model of the fabric. The fabric used for the analysis of the hypar was a TYPE II fabric with elastic moduli of 670kN/m(warp) and 300kN/m(weft) and tensile strengths of 88kN/m(warp) and 79kN/m(weft). A uniform prestress of 2kN/m was prescribed over the whole of the roof fabric. Patch loads varying from -1.0kPa to 1.0kPa were applied separately on a high and a low patch of the hypar. Reactions at each of the corners (Fig.2) were obtained and plotted against the patch loads. Figure 4 is a sample of these plots. From the results, reactions at each corner due to unit positive or negative patch loads at each patch could be worked out by symmetry, thus giving the influence coefficients for the support reactions. It must be noted here that the load effect for these influence coefficients is actually the change in support reactions from the prestress condition due to the applied loads because even with no applied load, support reaction forces still exist due to prestress. Thus, if

pressure p(kPa) on a patch of area A causes support reactions R_p, then the influence coefficient ß can be defined as

$$ß = \frac{R_p - R_{0.0}}{A * p} \qquad .....(1)$$

p=±0.2 if the influence coefficients are defined at the level of realistic wind loads

This equation implies that the change in support reactions varies linearly with the applied load. As can be seen from Figure 4, this is a reasonable and conservative approximation for most support reactions. Due to the geometric non-linearity in the behaviour of the structure, the assumption that superposition applies is not totally accurate either.

The stiffness matrix for the structure was obtained and used to evaluate the natural frequencies of the whole prototype. The lowest or fundamental frequency of the prototype was found to be almost 3Hz which is well above the energy containing frequency of fluctuating wind, so there is little danger of lock-in leading to instability. This confirms that the prototype is sufficiently stiff and small to be considered a static structure.

4 Estimation of Peak Reactions Using Quasi-Steady and Covariance Integration Theory

The results of the wind tunnel tests and the structural analysis were combined to estimate the peak reactions at the corner supports. Most wind codes recommend the use of a quasi-steady design approach for determining peak wind loads on static low-rise structures. That is, peak pressures are obtained by multiplying mean pressure coefficients by the eaves height dynamic pressure due to gust wind velocity. This implies that fluctuating pressures depend entirely on upwind fluctuating velocity. Pressure fluctuations are assumed to be perfectly correlated everywhere.

The covariance integration method, developed by Holmes and Best [2], takes into account the correlation of pressures between different points or sections of a structure. Therefore, a more accurate description of the fluctuating pressure distribution over a structure is sought.

The varying load effects are obtained from the varying pressures using the influence coefficients ß such that

Load effect $$L(t)=\int_A p(t)ß\, dA \qquad .....(2)$$

Coefficient of load effect $$C_L(t)= \frac{L(t)}{½\rho \bar{U}^2 A} \qquad .....(3)$$

The mean load effect coefficient can then be written as

$$[\bar{C}_L]=[ß_i][\bar{C}_{pi}] \qquad .....(4)$$

in matrix form for discretised pressures (patch pressures)

$ß_i$= influence coefficient for load effect due to pressure on general patch i

C_{pi}= mean pressure coefficient (referenced to eaves dynamic pressure) on general patch i

Quasi steady theory then estimates the peak load effect coefficient as

$$\hat{C}_L = \bar{C}_L * G_u^2 \qquad .....(5)$$

where G_u, the gust factor, was measured as 2.03

Covariance integration estimates the variance of the load effect coefficient as

$$\sigma^2_{CL} = [\beta^T]\,[\sigma_{Cp}]\,[r]\,[\sigma_{Cp}]\,[\beta] \qquad .....(6)$$

r = normalised cross-correlation of pressure coefficients
σ_{Cp}= standard deviation of pressure coefficients at each location

and the peak load effect coefficient as

$$\hat{C}_L = \bar{C}_L + g\,\sigma_{CL} \qquad .....(7)$$

g = statistical peak factor (measured as ≈4 for low-rise structures by Holmes [2])

The matrix calculations above were used to estimate the peak reaction coefficients for the tension membrane hypar roof. The results are summarised in Table 1 which compares the quasi-steady and covariance integration estimates of peak support reaction coefficients for each support for several wind directions. For the most part, the covariance integration estimates were found to be larger than the quasi-steady estimates. This is surprising given that quasi-steady theory makes the very conservative assumption that peak pressures occur everywhere simultaneously. The measured cross correlation coefficient values are certainly small due to the different flow mechanisms on the roof. However, the standard deviation pressure coefficients are all very high. This appears to be the main reason behind the large covariance integration peak estimates. It should be noted here that quasi-steady theory fails when dealing with very small coefficient values, so not all the comparisons in Table 1 are valid. Ideally, also, the statistical peak value g should have been determined by analysing the time history of the pressure fluctuations.

5 Conclusions

The mean and fluctuating pressure distributions over a typical hypar roof have been obtained from a wind tunnel study. Analysis of the results indicate that covariance integration, although much more sophisticated, produces similar estimates of peak load effects as the quasi-steady method for the tension membrane hypar. There would be some logic in this given the non-linearity of the structure's response to applied load. However, this conclusion has to be qualified by noting that the unusually high RMS coefficients measured substantially increased the covariance integration estimates. Tests using a larger model may help clarify these RMS pressures.

6 References

1 J.L. Meek and P.T.S. Ho, 'SHAPE: (A membrane shape-finding program for tension structures)', Adv. Eng. Software,v7 n1 (1985) 2-7

2 J.D. Holmes and R.J. Best, 'An approach to the determination of wind load effects on low rise buildings', J. Wind Eng. Ind. Aerodyn., 7 (1981) 273-287

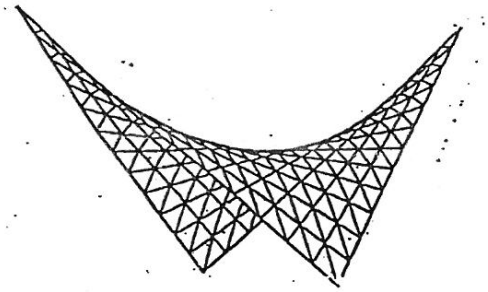

Fig.1 The hyperbolic paraboloid

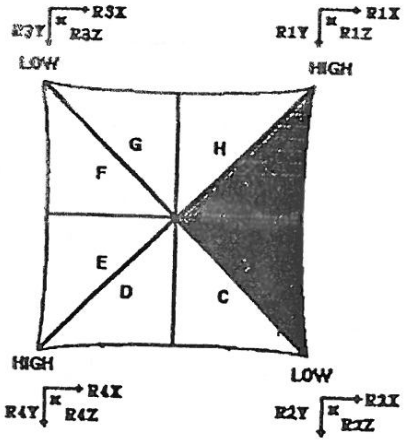

Fig.2 Model patch divisions and support reactions

PANEL PRESSURES -
SINGLE HYPAR .NO BLOCKAGE

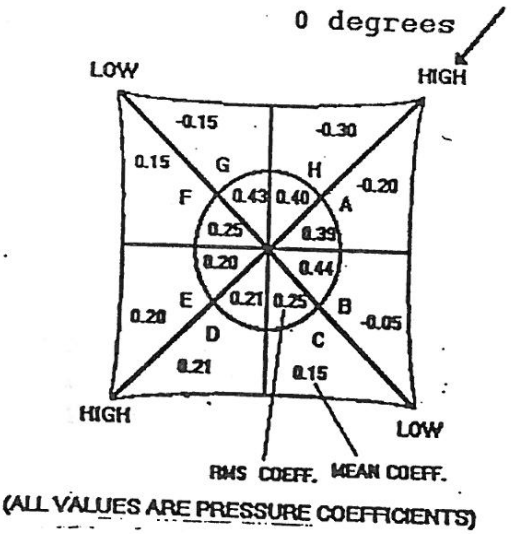

(ALL VALUES ARE PRESSURE COEFFICIENTS)

CROSS CORRELATION COEFFICIENTS

ANGLE OF ATTACK- 0 DEGREES

	A	B	C	D	E	F	G	H
A	1.00	0.63	0.57	0.47	0.43	0.49	0.51	0.57
B		1.00	0.72	0.41	0.36	0.31	0.26	0.34
C			1.00	0.43	0.39	0.34	0.28	0.29
D				1.00	0.35	0.35	0.28	0.24
E					1.00	0.33	0.27	0.26
F						1.00	0.51	0.37
G							1.00	0.47
H								1.00

PANEL PRESSURES -
SINGLE HYPAR .NO BLOCKAGE

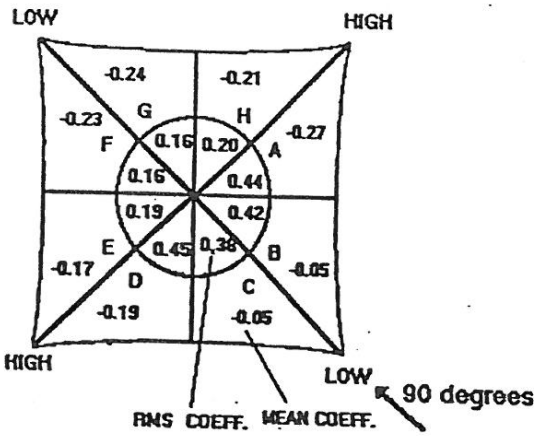

(ALL VALUES ARE PRESSURE COEFFICIENTS)

CROSS CORRELATION COEFFICIENTS

ANGLE OF ATTACK- 90 DEGREES

	A	B	C	D	E	F	G	H
A	1.00	0.58	0.40	0.29	0.29	0.11	0.10	0.65
B		1.00	0.61	0.45	0.42	0.17	0.13	0.50
C			1.00	0.62	0.51	0.13	0.19	0.44
D				1.00	0.66	0.10	0.14	0.31
E					1.00	0.17	0.18	0.28
F						1.00	0.32	0.23
G							1.00	0.23
H								1.00

Fig.3 Sample wind tunnel test results

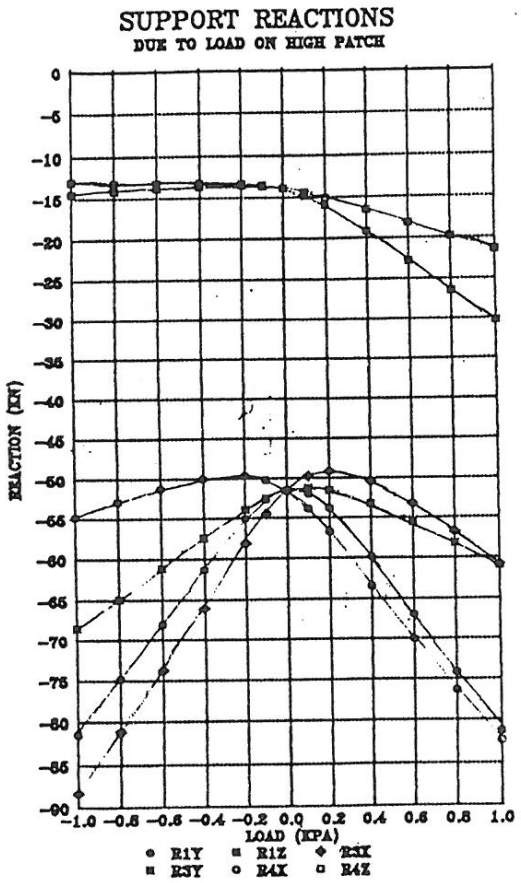

Fig.4 Sample structural analysis results

ANGLE (DEGS)	REACT.	MEAN COEF	VAR COEF	PEAK COEF COV INT	PEAK COEF Q-STEADY
0.0	R1X	1.2	0.5	3.9	5.0
	R1Y	-1.2	0.5	-4.0	-5.1
	R1Z	-0.1	0.1	-1.1	-0.6
	R2X	0.2	0.8	3.8	0.8
	R2Y	1.2	3.2	8.4	5.0
	R2Z	0.2	0.4	2.7	0.7
	R3X	-1.2	3.3	-8.4	-4.8
	R3Y	-0.1	0.9	-3.9	-0.4
	R3Z	0.2	0.4	2.7	0.9
	R4X	-0.2	0.4	-2.7	-0.6
	R4Y	0.1	0.3	2.4	0.2
	R4Z	-0.2	0.1	-1.6	-1.0
45.	R1X	0.6	0.2	2.6	2.6
	R1Y	-0.8	0.6	-3.8	-3.1
	R1Z	0.1	0.1	1.5	0.3
	R2X	0.6	0.4	3.0	2.5
	R2Y	1.4	1.3	5.9	5.8
	R2Z	0.3	0.3	2.4	1.4
	R3X	-1.3	2.5	-7.6	-5.2
	R3Y	-0.4	1.1	-4.7	-1.8
	R3Z	0.4	0.2	2.3	1.6
	R4X	0.1	1.1	4.3	0.3
	R4Y	-0.2	0.2	-1.8	-0.9
	R4Z	0.1	0.1	1.5	0.2
90.	R1X	0.3	0.5	3.1	1.4
	R1Y	-0.5	0.3	-2.8	-2.0
	R1Z	0.1	0.0	0.7	0.5
	R2X	1.4	2.5	7.7	5.9
	R2Y	1.6	2.5	8.0	6.6
	R2Z	0.5	0.6	3.7	2.2
	R3X	-1.4	3.6	-9.	-5.8
	R3Y	-1.3	3.6	-8.8	-5.2
	R3Z	0.6	0.4	3.1	2.6
	R4X	-0.3	0.3	-2.6	-1.4
	R4Y	0.2	0.5	2.9	0.8
	R4Z	0.1	0.0	0.7	0.5

Table 1 Comparison of peak reaction coefficients
(Covariance integration vs Quasi-steady)